NASA/TM–2013-218038

UV Lidar Receiver Analysis for Tropospheric Sensing of Ozone

Denis Pliutau
Science Systems and Applications, Inc., Hampton, Virginia

Russell J. DeYoung
Langley Research Center, Hampton, Virginia

August 2013

NASA STI Program . . . in Profile

Since its founding, NASA has been dedicated to the advancement of aeronautics and space science. The NASA scientific and technical information (STI) program plays a key part in helping NASA maintain this important role.

The NASA STI program operates under the auspices of the Agency Chief Information Officer. It collects, organizes, provides for archiving, and disseminates NASA's STI. The NASA STI program provides access to the NASA Aeronautics and Space Database and its public interface, the NASA Technical Report Server, thus providing one of the largest collections of aeronautical and space science STI in the world. Results are published in both non-NASA channels and by NASA in the NASA STI Report Series, which includes the following report types:

- TECHNICAL PUBLICATION. Reports of completed research or a major significant phase of research that present the results of NASA Programs and include extensive data or theoretical analysis. Includes compilations of significant scientific and technical data and information deemed to be of continuing reference value. NASA counterpart of peer-reviewed formal professional papers, but having less stringent limitations on manuscript length and extent of graphic presentations.

- TECHNICAL MEMORANDUM. Scientific and technical findings that are preliminary or of specialized interest, e.g., quick release reports, working papers, and bibliographies that contain minimal annotation. Does not contain extensive analysis.

- CONTRACTOR REPORT. Scientific and technical findings by NASA-sponsored contractors and grantees.

- CONFERENCE PUBLICATION. Collected papers from scientific and technical conferences, symposia, seminars, or other meetings sponsored or co-sponsored by NASA.

- SPECIAL PUBLICATION. Scientific, technical, or historical information from NASA programs, projects, and missions, often concerned with subjects having substantial public interest.

- TECHNICAL TRANSLATION. English-language translations of foreign scientific and technical material pertinent to NASA's mission.

Specialized services also include organizing and publishing research results, distributing specialized research announcements and feeds, providing information desk and personal search support, and enabling data exchange services.

For more information about the NASA STI program, see the following:

- Access the NASA STI program home page at *http://www.sti.nasa.gov*

- E-mail your question to help@sti.nasa.gov

- Fax your question to the NASA STI Information Desk at 443-757-5803

- Phone the NASA STI Information Desk at 443-757-5802

- Write to:
  STI Information Desk
  NASA Center for AeroSpace Information
  7115 Standard Drive
  Hanover, MD 21076-1320

NASA/TM–2013-218038

UV Lidar Receiver Analysis for Tropospheric Sensing of Ozone

Denis Pliutau
Science Systems and Applications, Inc., Hampton, Virginia

Russell J. DeYoung
Langley Research Center, Hampton, Virginia

National Aeronautics and
Space Administration

Langley Research Center
Hampton, Virginia 23681-2199

August 2013

Available from:

NASA Center for AeroSpace Information
7115 Standard Drive
Hanover, MD 21076-1320
443-757-5802

Abstract

A simulation of a ground based Ultra-Violet Differential Absorption Lidar (UV-DIAL) receiver system was performed under realistic daytime conditions to understand how range and lidar performance can be improved for a given UV pulse laser energy. Calculations were also performed for an aerosol channel transmitting at 3 W. The lidar receiver simulation studies were optimized for the purpose of tropospheric ozone measurements. The transmitted lidar UV measurements were from 285 to 295 nm and the aerosol channel was 527-nm. The calculations are based on atmospheric transmission given by the HITRAN database and the Modern Era Retrospective Analysis for Research and Applications (MERRA) meteorological data. The aerosol attenuation is estimated using both the BACKSCAT 4.0 code as well as data collected during the CALIPSO mission. The lidar performance is estimated for both diffuse-irradiance free cases corresponding to nighttime operation as well as the daytime diffuse scattered radiation component based on previously reported experimental data. This analysis presets calculations of the UV-DIAL receiver ozone and aerosol measurement range as a function of sky irradiance, filter bandwidth and laser transmitted UV and 527-nm energy.

1. Introduction

Ozone lidar systems consist basically of two components: a laser transmitter and an optical receiver. For the detection of ozone in the atmosphere from ground based lidars, laser wavelengths from 280-310 nm are used as these wavelengths correspond to a high absorption cross-section of the ozone molecule. A laser transmitter must transmit two or more UV wavelengths at high energy and short pulse length to achieve maximum ozone measurement range in the atmosphere. Also, for maximum ozone measurement range, the receiver telescope must be as large as possible and the detection system must operate at high optical efficiency.

Laser transmitters consistently have been the most difficult and unreliable components of the lidar system. The laser is susceptible to optical damage and degradation over time due to the high UV pulse energy and which limits the laser pulse energy transmitted into the atmosphere. Laser transmitters tend to be very costly thus simply increasing laser pulse energy has cost limitations.

Conversely, the lidar receiver is much less costly and does not suffer from optical damage. Thus, in order to optimize ozone lidar performance it is most cost effective to improve the performance of the receiver, as opposed to increasing the transmitted laser energy, by collecting every backscattered lidar photon with high efficiency. High efficiency can be achieved by using a large area telescope and a high optical efficiency detection subsystem.

The objective of this paper is to perform an analysis of a typical UV-DIAL lidar receiver system under realistic day and night time conditions to understand how range and lidar performance can be improved for a given UV pulse laser energy for the ozone and 527 nm aerosol retrieval [1]. Here we

describe simulation studies for lidar receiver optimization for the purpose of tropospheric ozone and aerosol measurements. The transmitted lidar measurements will be from 285 to 295 nm and the aerosol channel will be 527 nm.

2. Lidar receiver calculation overview

There are multiple components in a typical lidar setup affecting the accuracy and range of the lidar measurements. Lidar receiver calculations were carried out using a set of different modeling codes and datasets as shown in Fig. 1. As can be seen in Fig 1 the lidar equation, which gives the power, P as a function of range r received for a given transmitted power, is used with the aerosol and molecular attenuation (α) and backscatter (β) and calculated using several alternative methods [2]. In particular, the molecular attenuation (α) is calculated using the cross-sectional data from the HITRAN database by using a set of data from the Modern Era Retrospective Analysis for Research and Applications (MERRA) dataset [3] [4]. The advantage of using the MERRA dataset is the ability to obtain meteorological parameters for specific locations, times of day and seasons, thus providing more exact transmission spectra for lidar locations of interest. In particular, annual averaged ozone concentration profiles were obtained using the MERRA "MERRA300.prod.assim.inst6_3d_ana_Nv" dataset for the Hampton, VA and Houston, TX locations where the UV-DIAL system under study is expected to be primarily deployed. The aerosol attenuation was estimated using an approach based on the use of the BACKSCAT 4.0 model [6] providing aerosols attenuation values as a function of altitude and wavelength for a set of seasonal variations and commonly encountered atmospheric aerosol types including the Rayleigh scattering component. A comparison of the BACLSCAT 4.0 aerosol profile with the "CAL_LID_L3_APro_AllSky-Beta-V1" data from the CALIPSO mission [5] is also presented for validation purposes.

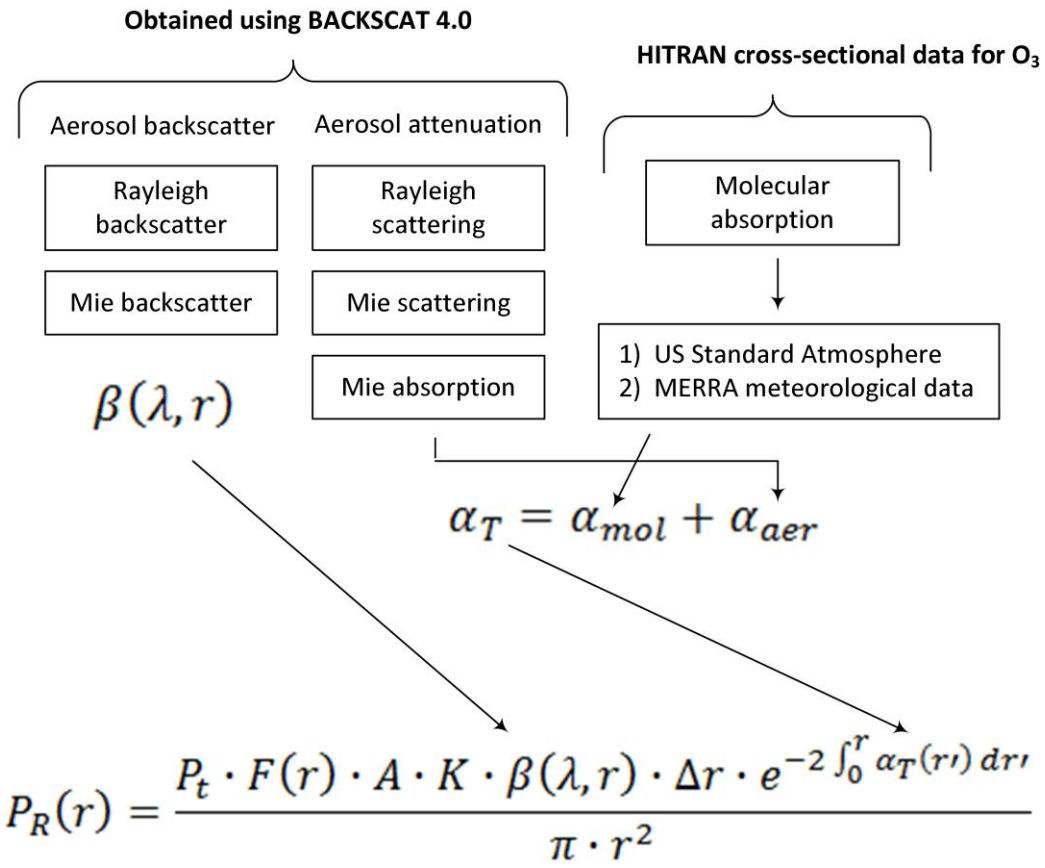

Fig 1. Overview of the lidar sensitivity analysis calculations. Where β(λ, r) is the aerosol backscatter coefficient as a function of wavelength and range, α_{mol} is the molecular attenuation , and α_{aer} is the total aerosol attenuation component.

3. Calculation of daytime diffuse sky irradiance background component

3.1 – Determining the diffuse sky irradiance at 290nm

To determine the optical performance of the lidar return, several noise sources must be considered. Of them the most important is the sky irradiance (W / m^2) within the optical bandwidth of the receiver. First, a diffuse spectrum of UV sky irradiance spectrum was found in the literature for the UV-B spectral region of interest near 290 nm [7]. As can be seen in the Fig 2 curve b spectrum, the diffuse irradiance without the ozone attenuation at the earth surface provides a value of about 0.15 W/ (m^2·nm) at 290 nm. The spectrum shown was obtained using a simulation model assuming a solar elevation angle of 35° (55° from zenith) [7]

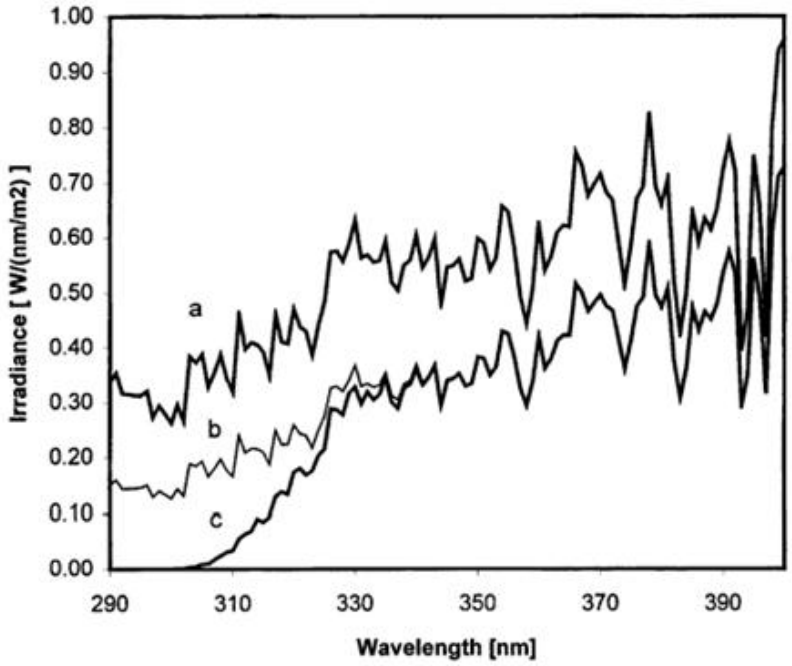

Fig 2 Modeled spectral irradiance for clear sky, no surface reflection and 35° solar elevation, ***a*** outside the atmosphere, ***b*** at the Earth's surface with no ozone in the atmosphere, ***c*** at the Earth's surface with 250 DU ozone abundance.

As can be seen from Figure 2 above, an irradiance difference between curve **b** and **c** at 310nm is equal to ~0.15W/(nm · m^2). In order to determine the value of the irradiance with the ozone attenuation taken into account the HITRAN cross-sectional data was used to determine the difference in absorption at 290 and 310 nm. It was found that the absorption by ozone at 290nm is up to 11 times (depending on the temperature range) stronger than at 310nm as can be seen from the ozone absorption spectra calculated for a horizontal path of 10km using HITRAN cross-sectional data at 300, 280, 260, 240, 220, and 200K shown in Figure 3 (the highest absorption is observed for the lowest temperature).

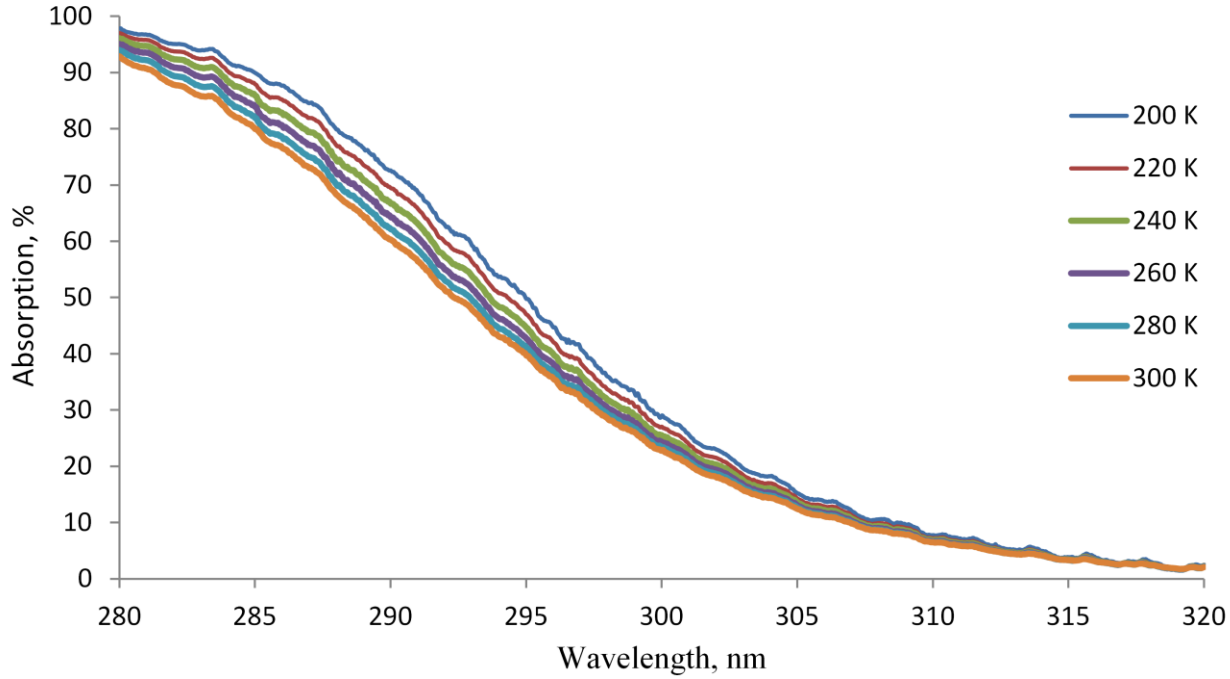

Fig 3. Molecular absorption curves of O_3 calculated using the HITRAN cross-sectional data for different temperatures and 10km path length.

Table 1 summarizes the recalculated diffuse sky irradiance values obtained at ground level with the ozone attenuation taken into account. The second column in the Table 1 shows relative increase of ozone absorption at wavelengths shown in column 1 compared to the ozone absorption at 310 nm. These relative difference values were used to establish the diffuse sky irradiances shown in column 3 for the 285, 290, and 290 nm wavelengths from the irradiance value at 310 nm

Table 1 Adjustment of diffuse sky irradiances at different wavelengths using wavelength dependent ozone absorption values

Wavelength, nm	**Absorption relative difference (times), compared to that at 310 nm**	**Resultant diffuse irradiance at ground level, W / (m^2* nm)**
285	13	0.0029
290	11	0.0034
295	7	0.0054

As a first estimate it is reasonable to approximate the ozone absorption curve in the 10 nm band pass filter region centered at 290 nm as a straight line as seen from the ozone simulation spectra of Fig. 3. Taking this into account, the averaged diffuse 290 nm sky irradiance value in the 10 nm spectral region of interest will approximately average to **0.0034 W / (m^2·nm)** at 290 nm. This value is comparable to the

measured values in the range of **$9.822 \cdot 10^{-5}$ – $2.022 \cdot 10^{-3}$ W / ($m^2 \cdot$nm)** at 295 nm reported for a location in Orlando, FL [8]. In our calculations we will not be using the values from [8] because they do not provide the information about the sun elevation angle at the time the measurements took place.

3.2 – Adjusting the irradiances for Sun angle

The value obtained in the previous section 3.1 is for the sun zenith angle of 55°. To adjust this value for other elevations we use the data from [8]. Figure 4 from [9] provides an example of integrated diffuse sky irradiance for a selected day as a function of sun zenith angle.

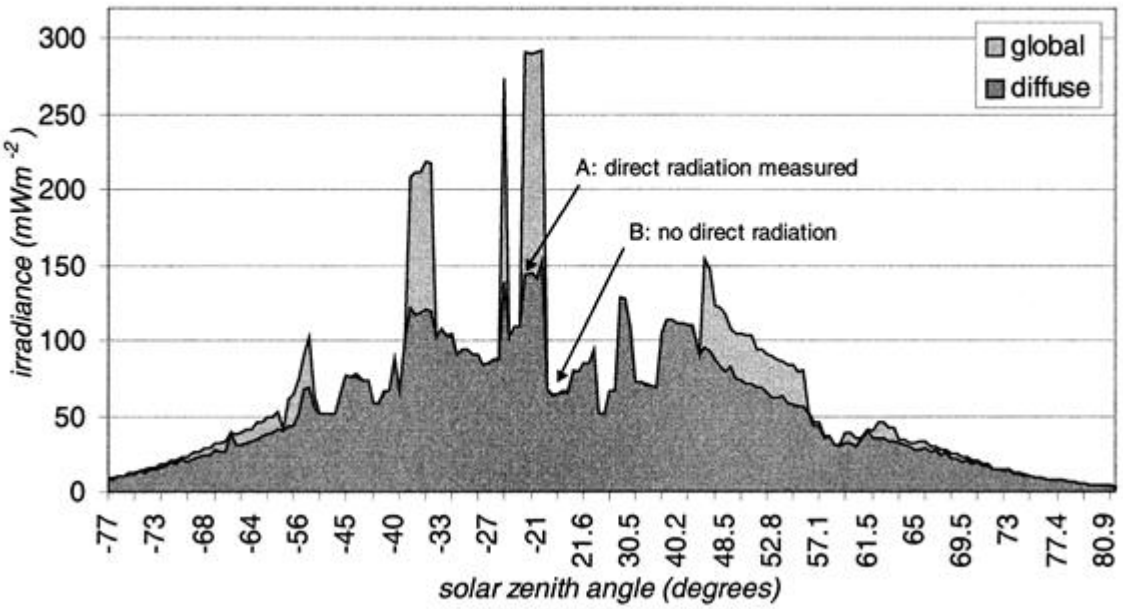

Fig 4. Variable sky-view diffuse irradiance superimposed on global irradiance for a cloudy sky day (6 Dec. 2000, 5-octa cumulus). From Ref. [9]

As can be seen, the diffuse irradiance values are about 3 times higher at their maximum compared to values at +/-55° zenith angles. To take this into account we increase the estimated 290 nm irradiance accordingly to obtain **0.01 W/ (m^2 * nm).** It should be pointed out that the data provided here is for a cloudy day; however, since we are interested in a relative increase of diffuse sky irradiance due to sun angle change, it is assumed that a clear sunny day would result in comparable results.

3.3 – Background light registered by the receiver for filter attenuation and bandwidth

The receiver is assumed to have a filter transmission curve with a HWHM of 10 nm centered at 290 nm and a transmission of 50% at the UV wavelengths. Thus the 290 nm irradiance value calculated previously is multiplied by 10 to adjust for the filter spectral bandwidth of 10 nm. Using this approach the irradiance value is **0.1 W / m^2** with the filter spectral transmission width taken into account.

Additionally, the value should be adjusted for the assumed transmission of the filter of 50% to get a value of **0.05 W / m^2**.

3.4 – Determining the field of view of the lidar telescope

Since we are dealing with diffuse light, the diffuse sky irradiance value has to be reduced by the ratio of the lidar steradian corresponding to the field of view (FOV) referenced to the entire half sphere representing the entire sky. In doing so it is assumed that diffuse irradiance components directed from different directions in the sky contribute equivalent amounts of irradiance. Equation 1 defines the sky diffuse power

$$P_{sky\ diffuse} = \frac{sr_{tele}}{sr_{half\ sphere}} \cdot I_{surf}^{wl} \cdot A \tag{1}$$

where $P_{sky\ diffuse}$ is the power registered by the receiver due to the diffuse sky irradiance, sr_{tele} is the steradian angle of the sky covered by the telescope, $sr_{half\ sphere}$ is the half sphere steradian angle, and I_{surf}^{wl} is the sky diffuse irradiance corrected for the presence of the optical filter, and A is the area of the telescope. The conversion between the FOV angle and steradian for small angles is as follows:

$$sr_{tele} = 2\pi(1-\cos(\theta_{FOV} \cdot 0.5)) \approx \pi(\theta_{FOV} \cdot 0.5)^2 \tag{2}$$

Taking into account the equation for the calculation of the field of view [10]:

$$\theta_{FOV} \cdot 0.5 = \arctan\left(\frac{\delta}{2f}\right) \tag{3}$$

where δ is the diameter of the field stop, and f is the focal length of the primary telescope mirror. The **FOV total angle of 0.001** for a field stop of 1mm and a telescope focal length of 1m corresponding to the parameters of the lidar telescope used in the UV-DIAL ozone lidar system. By using the calculated FOV angle, the value of sr_{tele} is thus equal to 7.85x10^{-7}.

3.5 - Calculating the detected diffuse sky irradiance at 290 nm

Taking the averaged diffuse sky irradiance value of **0.05 W / m**^{2} and adjusting it for the telescope field of view and the telescope surface area A we get:

$$P_{sky\ diffuse} = \frac{sr_{tele}}{sr_{half\ sphere}} \cdot I_{surf}^{wl} \cdot A = \frac{7.85 \times 10^{-7}}{2\pi} \cdot (0.05) \cdot (0.126) \approx 7.6 \times 10^{-10} Watt \qquad (4)$$

3.6 – Sky diffuse radiance estimates for the 527 nm lidar aerosol channel

The calculations for the 527 nm aerosol channel are similar to those shown above for the 290 nm channel. However, it is not necessary to establish the radiance level at 527 nm through scaling because the diffuse scattering data is widely available in the literature for this visible wavelength. In a similar fashion, literature reported spectra shown in Figure 5 were used to estimate the radiance levels in the 527 nm band. The spectra shown in Figure 5 were adopted from Ref. 11.

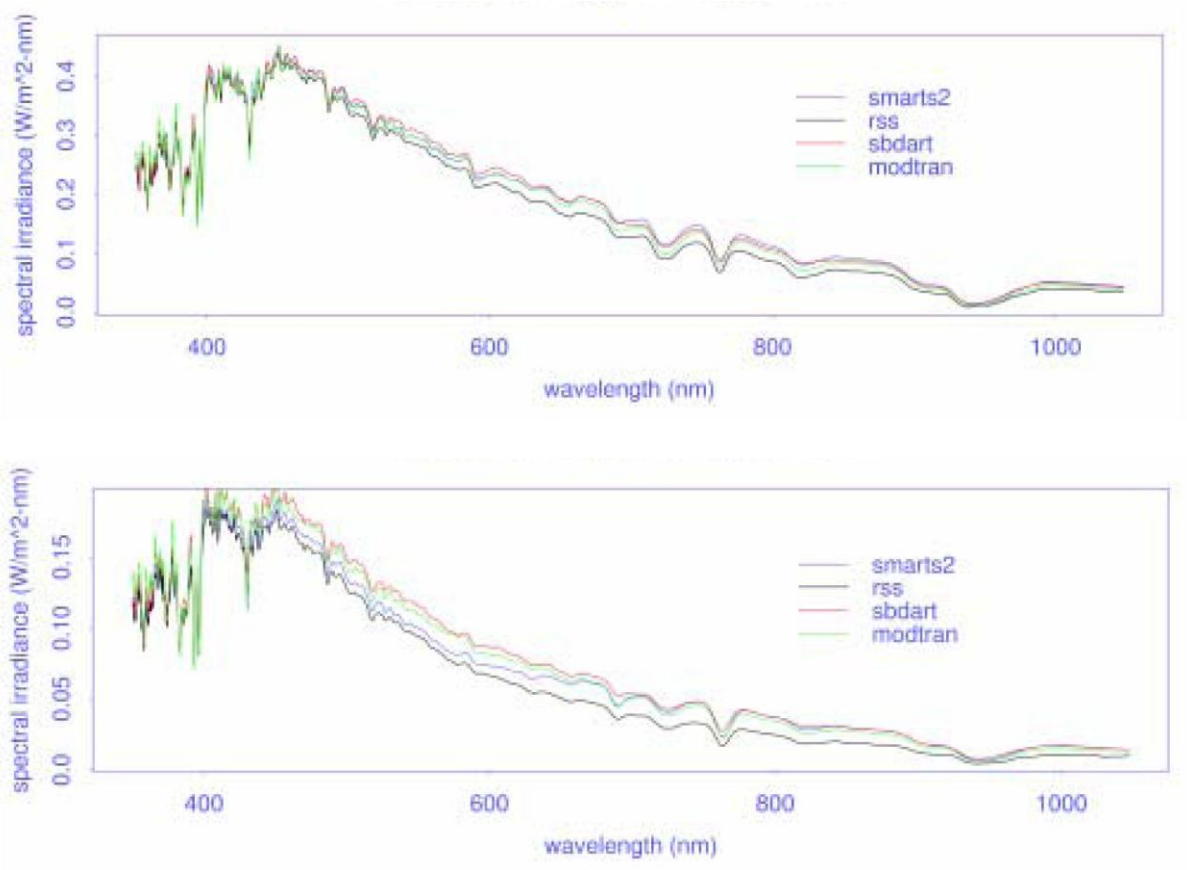

Fig. 5. Measured and modeled diffuse irradiance spectra for a humid hazy October day (top), and for a dry clear October day (bottom). Here rss stands for Rotating Shadowband Spectroradiometer. smarts2, sbdart and modtran are modeling codes [11].

The spectra above are for a hazy (top) and clear (bottom) day respectively showing diffuse irradiance values in the range **of 0.1 – 0.35 W / (m^2 * nm)**. After the adjustment for the filter HWHM bandwidth of

0.3nm we get irradiance values of **0.033 – 0.117 W / m^2**. Additional adjustment for the filter transmission of **40%** gives values of **0.0132 – 0.0468 W / m^2**. Taking the maximum value of **0.0468 W / m^2** and adjusting it for the telescope field of view and the telescope surface area we get the collected diffuse sky irradiance power from Eq. 5:

$$P_{sky\ diffuse} = \frac{sr_{tele}}{sr_{half\ sphere}} \cdot I_{surf}^{wl} \cdot A = \frac{7.85 \times 10^{-7}}{2\pi} \cdot 0.0468 \cdot 0.126 \approx 7.4 \times 10^{-10} Watt \qquad (5)$$

4. Calculation of the PMT Noise Equivalent Power (NEP)

A photo detector multiplier tube (PMT) commonly used in UV-DIAL lidar receivers is the Hamamatsu R7400-U03. These PMT characteristics were used to estimate the PMT detector noise level to establish the best achievable sensitivity and the maximum lidar detection range in the absence of any ambient light background signal contamination. The parameters for the PMT being used in the lidar system are summarized in Table 2.

Table 2 Parameters for the R7400-U03 photomultiplier tube.

Parameter	**Value**
Peak absorption	420 nm
Cathode sensitivity at peak 420 nm	62 mA/W
Cathode sensitivity at 290nm	~40 mA/W
Anode dark current	0.2 to 2 nA
Maximum gain	7 x 10^5

The noise equivalent power (NEP) is the lowest power detectable by PMT and it limits the lidar measurement range. Using the parameters in the table, the NEP for a given PMT is shown in Eq. 6:

$$NEP = \frac{i_n}{R_a} \cdot \sqrt{\Delta f} = \frac{i_n}{S_{peak} \cdot G} \cdot \sqrt{\Delta f} = \frac{0.2\,nA}{40\frac{mA}{W} \cdot 7 \times 10^5} = 0.71 \times 10^{-11}\,W \qquad (6)$$

where i_n is the anode dark current, R_a is the anode sensitivity, Δf is the detector bandwidth assumed to be equal to 1MHz, S_{peak} is the peak cathode sensitivity, and G is the maximum gain of the PMT. Equation 7 takes into account the averaging of the signal over 20 seconds, so the NEP is reduced by a factor of $\sqrt{N}$, where N is the number of laser pulses in the averaging interval (assuming 1kHz repetition rate):

$$\sqrt{N} = \sqrt{20 \cdot 1000} \approx 141 \tag{7}$$

Equation 8 shows the adjusted NEP for the accumulation of spectra over 20 seconds as:

$$NEP_{20\,\mathrm{sec}} = \frac{0.71 \times 10^{-11} W}{141} \approx 0.5 \cdot 10^{-13} W \tag{8}$$

This NEP value is compared to the power vs. range spectrum obtained with the lidar simulation in section 5. It should be noted that the lowest anode dark current value was used in the calculations and there are obviously some additional noise factors in the data acquisition system.

5. Ozone atmospheric profiles for atmospheric transmission calculations

Atmospheric transmission calculations are now discussed using the ozone profile data extracted from the MERRA dataset [4] for the locations of Hampton, VA and Houston, TX with subsequent averaging to obtain annual mean O_3 profiles suitable for the current lidar estimate calculations. The ozone atmospheric profiles extracted from the MERRA dataset are shown in Fig. 6. As can be seen, the ozone profiles extracted from MERRA account for ozone fluxes near the ground which makes them more suitable for the tropospheric ozone lidar estimate calculations than the US standard profile [12] of ozone shown in the left figure.

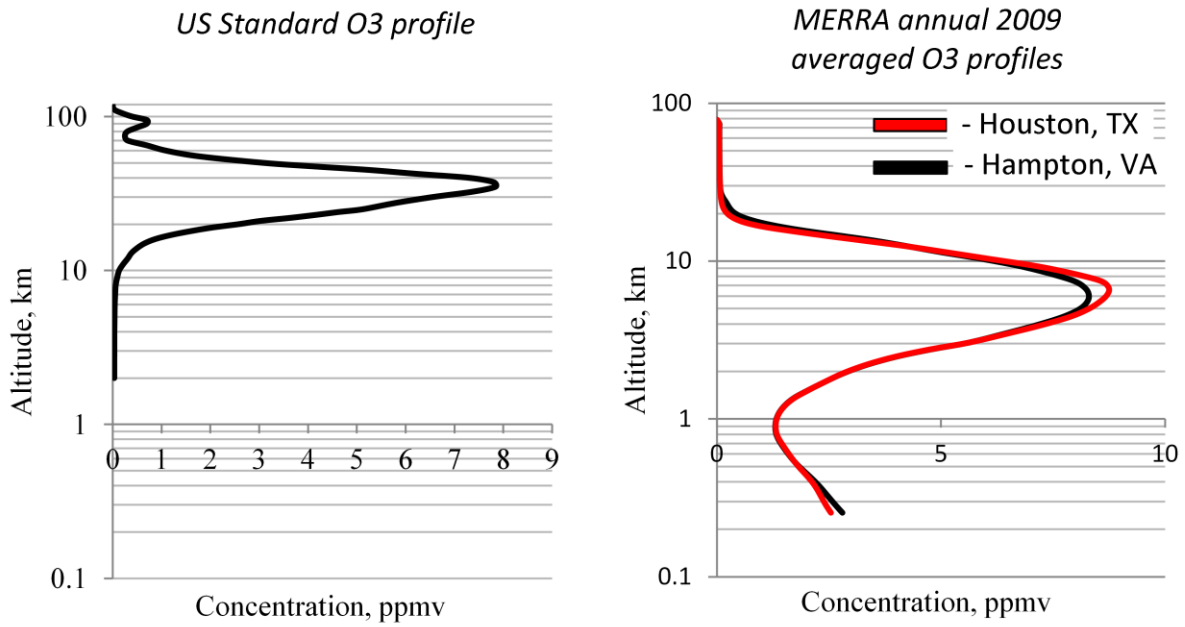

Fig. 6. O_3 atmospheric profiles from the US Standard model (left), and annual mean for year 2009 of the MERRA O_3 profile data near Hampton VA and Houston TX locations.

Additionally, the overall shape of the ozone profiles retrieved from the MERRA dataset is different from that in the US Standard model with the maximum ozone mixing ratio peak shifted toward the ground which is of importance for tropospheric lidar sensitivity estimates. Our further lidar calculations are thus based only on the MERRA atmospheric profiles.

6. Aerosol 290 nm attenuation and backscatter calculations using the BACKSCAT 4.0 lidar program

The aerosol calculations were carried out using the BACKSCAT 4.0 program [6] using the parameters shown in Fig. 7.

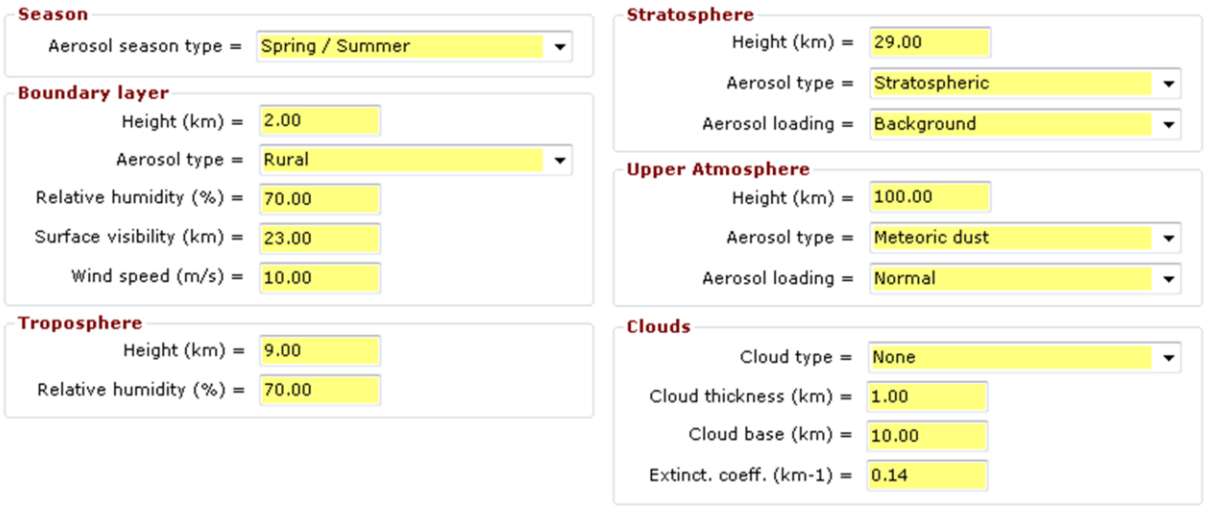

Fig. 7. Aerosol profile characteristics used in the BACKSCAT 4.0 program for the aerosol calculations.

As can be seen from Fig. 7, "Rural" aerosol type is used in the calculations because it provides higher values of the aerosol attenuation and backscatter values compared to the "Urban" type also available in the BACKSCAT 4.0 model. The results of aerosol calculations including the attenuation and backscatter data at 290nm as a function of altitude are presented in Fig. 8 showing individual aerosol attenuation (left) and backscatter components (right) as well as their totals.

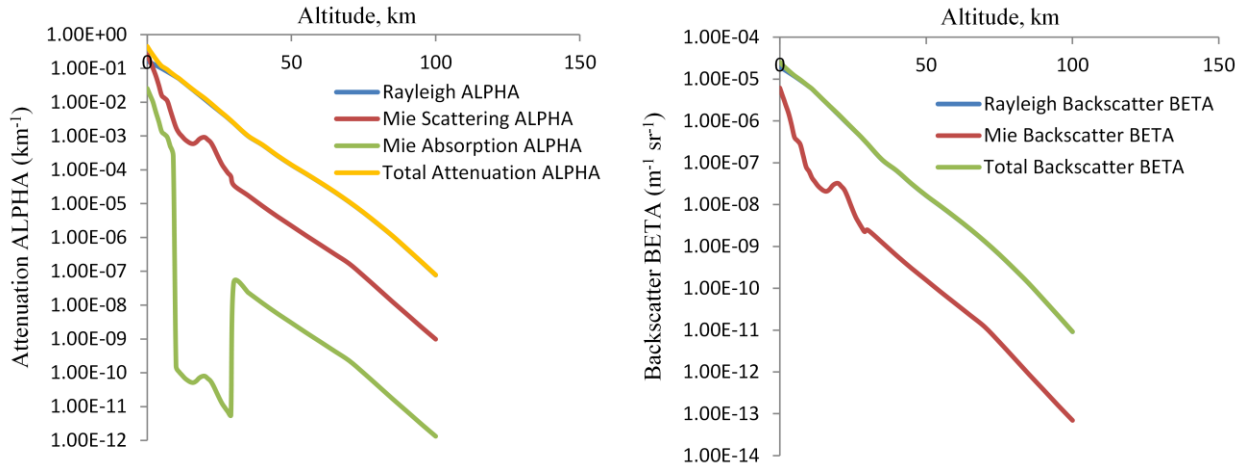

Fig. 8. Aerosol absorption (left) and backscatter (right) calculations at 290 nm using the BACKSCAT 4.0 program.

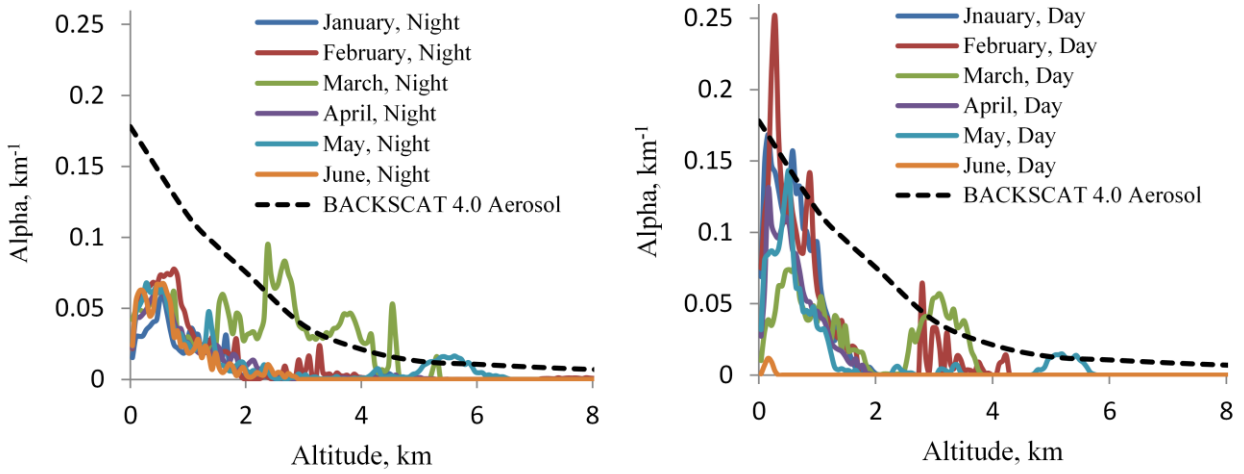

Fig. 9. Comparison of the CALIPSO monthly averaged aerosol day and night extinction profiles for year 2009 at Hampton, VA (colored lines) with the aerosol profile generated using the BACKSCAT 4.0 program (dashed file) at 532 nm.

To further verify the applicability of the aerosol attenuation data available using the BACLSCAT 4.0 model we have carried out a comparison of the total aerosol attenuation (extinction) profiles at 532 nm generated using the BACKSCAT 4.0 program with the profiles obtained during the CALIPSO mission. Such a comparison is presented in Fig. 9 where daytime and nighttime monthly January through June of 2009 aerosol extinction averages are compared to those obtained using the BACKSCAT 4.0 program with parameters shown in Fig. 7 As can be seen, the BACKSCAT 4.0 attenuation data represents a realistic estimated aerosol extinction value even though the atmospheric aerosol concentration is highly variable. The results of the BACKSCAT 4.0 program calculations are used in our simulations for the wavelengths of 290 and 527 nm.

7. Ozone lidar calculation results

The estimates of the daytime diffuse sky irradiance shown in Section 3 and the detector noise level estimates described in Section 4 limit the maximum detectable range of the lidar system for the realistic daytime and nighttime lidar operation cases respectively.

Table 3 Lidar system parameters used to calculate the ozone sensitivity, aerosol retrieval and maximum range

Parameter	285-295nm lidar (ozone)	527nm lidar (aerosol)
Pulse energy	0.1 – 1 mJ	3mJ
Pulse duration	100ns	
Laser wavelength	290nm	527nm
Bandwidth	5MHz	
Telescope diameter	40 cm	
Lidar system efficiency	40%	

In this section we perform lidar return calculations by using the lidar system parameters presented in Table 3 and the molecular and aerosols absorption and backscatter values calculated as described in the previous sections. Previous calculations of detector and diffuse sky irradiance estimates are combined to establish the maximum estimated range achievable with the given lidar system parameters.

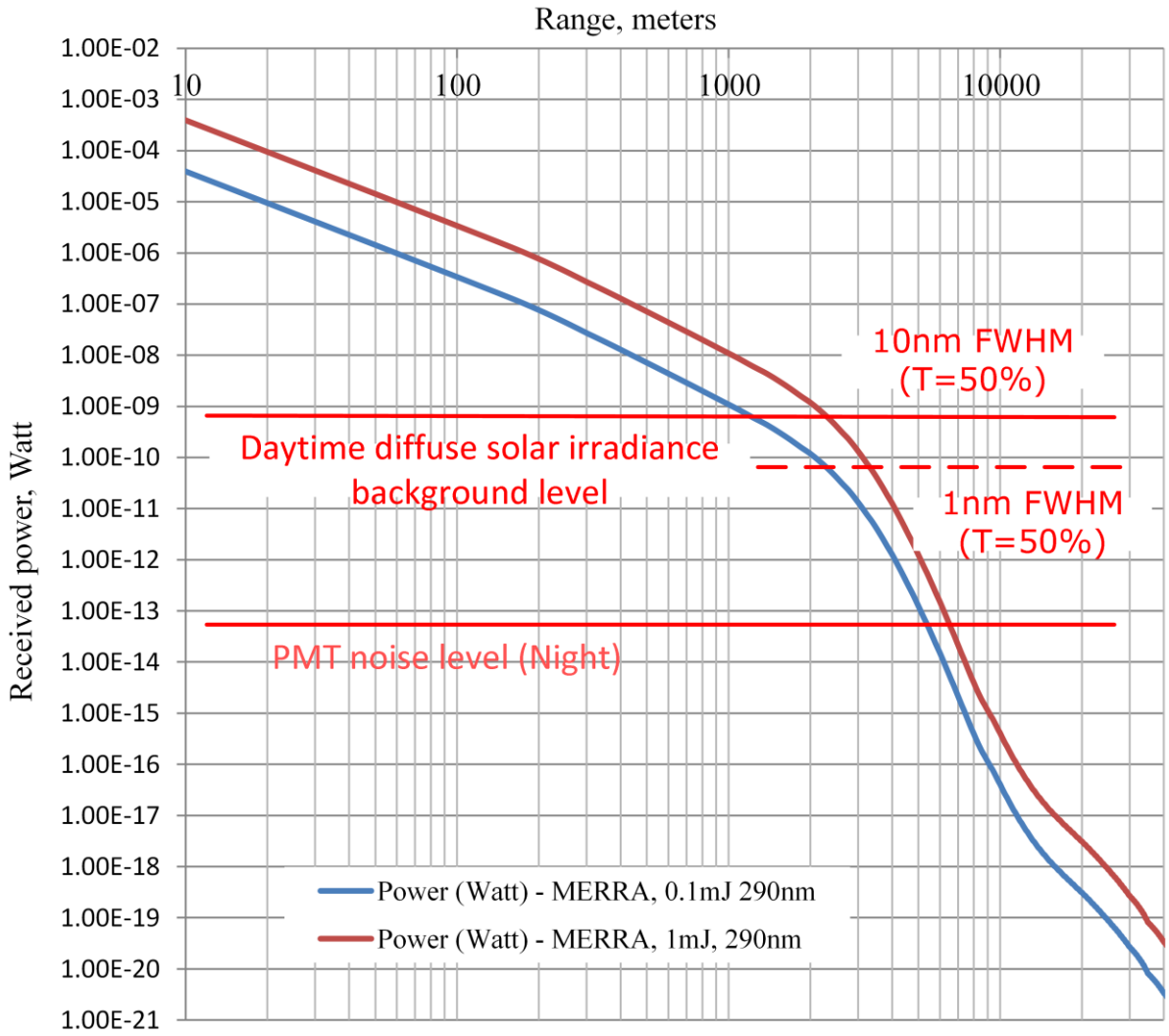

Fig 10. Logarithmic plot of lidar return analysis at 290nm using MERRA ozone concentration profiles at 2 different output laser energy levels of 0.1mJ and 1 mJ. The PMT noise level is a 20s (20000 laser pulses) averaged value and represents the estimated nighttime range.

Figure 10 presents the results of the lidar analysis for the measurement of ozone concentration in the troposphere using different atmospheric ozone profiles described in Section 5. During daytime operation a maximum detectable range of 1 to 2.5 km is expected as the laser output pulse energy is increased from 0.1 mJ (0.1W) to 1 mJ (1 W) and during the nighttime operation the maximum range is increased to 5.5 to 6.5 km respectively. As can be seen the filter with 1nm FWHM (T = 50%) would results in an increase of the daytime maximum detectable range of 2.5 – 3.6 km respectively (dashed line).

8. Aerosol lidar calculation results

Lidar analysis was performed for the measurement of aerosols using the 527 nm laser wavelength to be transmitted simultaneously with the ozone measurements. The lidar system parameters used for the estimates are summarized in Table 3. The results of the lidar aerosol analysis are presented in Fig. 11. As can be seen, a range of over 3.5 km is achievable during the daytime and a maximum range of 35 km at nighttime in the absence of any ambient light interferences.

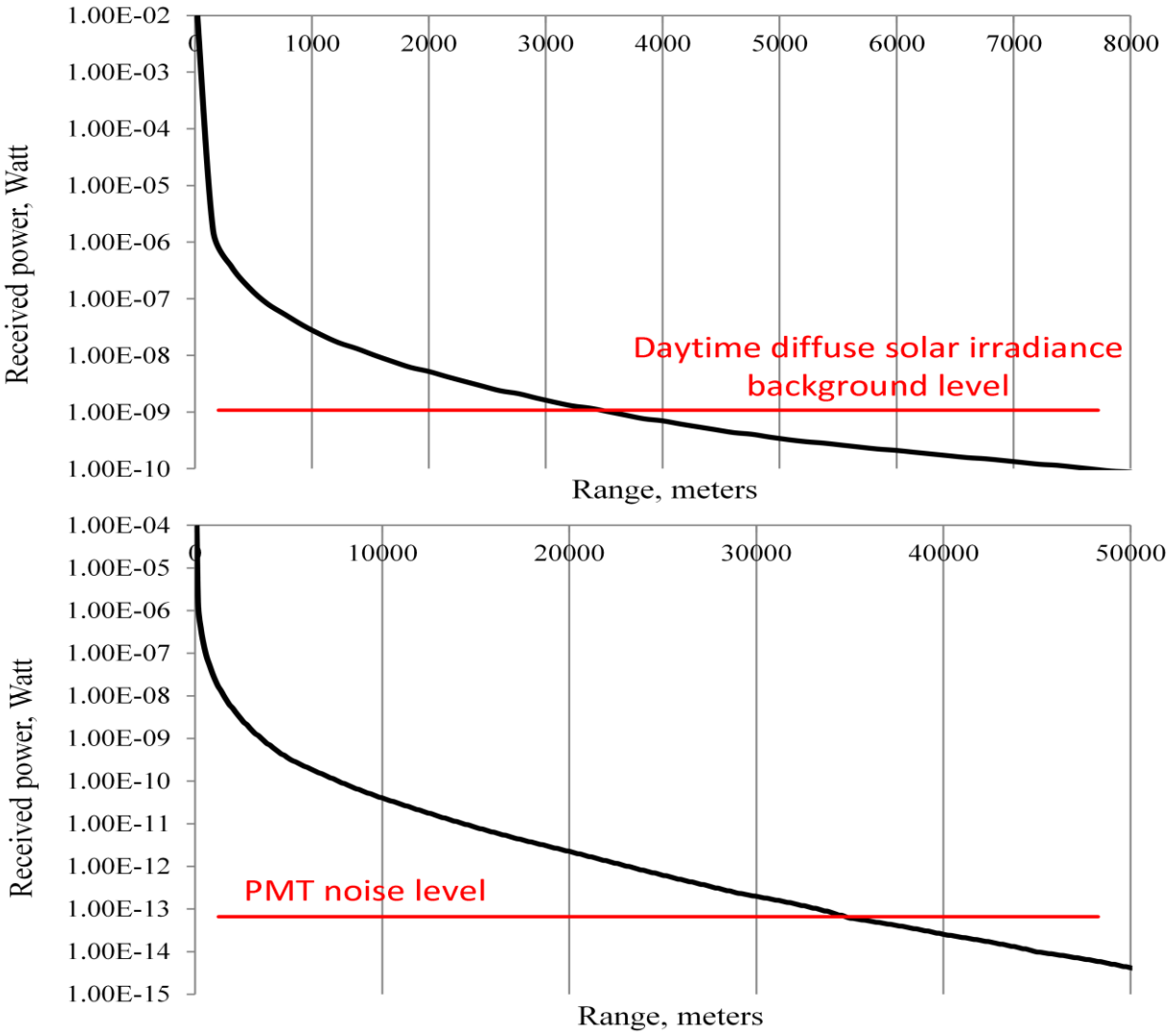

Fig. 11. Lidar sensitivity calculations for the measurements of aerosols at 527 nm with a laser energy of 3mJ per pulse. The PMT noise level is a 20s (20000 laser pulses) averaged value. The upper plot represents daytime operation and the lower plot represents nighttime operation.

9. Conclusions

Calculations were performed for a UV-DIAL ozone lidar system operating between 285-295 nm with laser energy between 0.1 and 1.0 mJ per pulse (1 kHz) and having a 527 nm aerosol channel transmitting at 3 W. The receiver has a 40 cm diameter telescope and a 10-nm FWHM (T = 50%) filter to cover the 285-295 nm laser transmission range. Under these conditions the daytime ozone measurement range was 1 - 2.5 km for the laser energy specified. For the aerosol channel the daytime range was 3.5km (3mJ / pulse). For nighttime operation the ozone measurement range is increased to 5 – 6 km for the given laser energies. A daytime limiting factor is the 10-nm FWHM optical filter. If a 1-nm tunable UV filter (T = 50%) could be designed and implemented, the daytime ozone measurement range could be increased to 2.5 – 3.5 km.

Acknowledgment

The authors are grateful for the support of Jack Kaye (NASA HQ) for funding this research under the Tropospheric Ozone Lidar Measurements Program.

References

[1] Viktor A. Fromzel, Coorg R. Prasad, Karina B. Petrosyan, Yishinn Liaw, Mikhail A. Yakshin, Wenhui Shi, and Russell DeYoung, "Tunable, Narrow Linewidth, High Repetition Frequency Ce:LiCAF Lasers Pumped by the Fourth Harmonic of a Diode-Pumped Nd:YLF Laser for Ozone DIAL Measurements", in Advances in Optical and Photonic Devices, Edited by Ki Young Kim, InTech, January 2010

[2] De Young, Russell, "Aircraft and Space Atmospheric Measurements Using Differential Absorption Lidar (DIAL)" in Earth System Monitoring, by Orcutt, John, ISBN 978-1-4614-5683-4. Springer Science+Business Media New York, 2013, p. 35

[3] L. S. Rothman, Iouli E. Gordon et al., "The HITRAN 2008 molecular spectroscopic database", JQSRT, 110, 533-572, (2009)

[4] Rienecker, M.M., M.J. Suarez, R. Gelaro, R. Todling, J. Bacmeister, E. Liu, M.G. Bosilovich, S.D. Schubert, L. Takacs, G.-K. Kim, S. Bloom, J. Chen, D. Collins, A. Conaty, A. da Silva, et al., **"** MERRA - NASA's Modern-Era Retrospective Analysis for Research and Applications"**,** *J. Climate,* 24, 3624-3648, 2011, doi: 10.1175/JCLI-D-11-00015.1

[5] David M. Winker ; Jacques R. Pelon ; M. Patrick McCormick; The CALIPSO mission: spaceborne lidar for observation of aerosols and clouds. Proc. SPIE 4893, 466539 (2003).

[6] David R Longtin, Michael G Cheifeiz, James R Jones, John F Hommel, "Backscat lidar simulation version 4.0: Technical documentation and users guide.", PL-TR-94-2170, 10 June 1994

[7] "UV Radiation and Arctic Ecosystems", by Dag Olav Hassen, Springer 2002, ISBN: 3540421068

[8] "The measurement of ultraviolet spectral irradiant problems and solutions", Optronic Laboratories, Inc., June, 1990

[9] Christopher Kuchinke and Manuel Nunez "A Variable Sky-View Platform for the Measurement of Ultraviolet Radiation", Journal of Atmospheric Technology, Vol. 20, pp. 1170 – 1182, (2003).

[10] Hiroaki Kuze, Hideki Kinjo, Yasushi Sakurada, and Nobuo Takeuchi, "Field-of-View Dependence of Lidar Signals by Use of Newtonian and Cassegrainian Telescopes," Appl. Opt. **37**, 3128-3132 (1998)

[11] J. J. Michalsky et al, "Shortwave, Clear-Sky Diffuse Irradiance in the 350 to 1050 nm Range: Comparison of Models with RSS Measurements at the Southern Great Plains ARM Site in September/October 2001", Thirteenth ARM Science Team Meeting Proceedings, Broomfield, Colorado, March 31-April 4, 2003

[12] G. P. Anderson, J. H. Chetwynd, S. A. Clough, E. P. Shettle, F. X. Kneizys, "AFGL Atmospheric Constituent Profiles (0-120km), AFGL-TR-86-0110, 15 May 1986

REPORT DOCUMENTATION PAGE

Form Approved
OMB No. 0704-0188

1. REPORT DATE *(DD-MM-YYYY)*	2. REPORT TYPE	3. DATES COVERED *(From - To)*
01- 08 - 2013	Technical Memorandum	

4. TITLE AND SUBTITLE

UV Lidar Receiver Analysis for Tropospheric Sensing of Ozone

5a. CONTRACT NUMBER

5b. GRANT NUMBER

5c. PROGRAM ELEMENT NUMBER

6. AUTHOR(S)

Pliutau, Denis; DeYoung, Russell J.

5d. PROJECT NUMBER

5e. TASK NUMBER

5f. WORK UNIT NUMBER

509496.02.08.05.07

7. PERFORMING ORGANIZATION NAME(S) AND ADDRESS(ES)

NASA Langley Research Center
Hampton, VA 23681-2199

8. PERFORMING ORGANIZATION REPORT NUMBER

L-20251

9. SPONSORING/MONITORING AGENCY NAME(S) AND ADDRESS(ES)

National Aeronautics and Space Administration
Washington, DC 20546-0001

10. SPONSOR/MONITOR'S ACRONYM(S)

NASA

11. SPONSOR/MONITOR'S REPORT NUMBER(S)

NASA/TM-2013-218038

12. DISTRIBUTION/AVAILABILITY STATEMENT

Unclassified - Unlimited
Subject Category 35
Availability: NASA CASI (443) 757-5802

13. SUPPLEMENTARY NOTES

14. ABSTRACT

Lidar calculations are presented pertaining to the measurement of O3 concentrations in the atmosphere using a ground-based Ultra-Violet Differential Absorption Lidar (UV-DIAL). The calculations are based on atmospheric transmission calculations using the HITRAN database and the Modern Era Retrospective Analysis for Research and Applications (MERRA) meteorological data. The aerosol attenuation is estimated using both the BACKSCAT 4.0 code as well as the data collected during the CALIPSO mission. The lidar performance is estimated for both diffuse-irradiance free cases corresponding to nighttime operation as well as the daytime diffuse scattered radiation component based on previously reported experimental data. This analysis presets calculations of the UV-DIAL receiver ozone measurement atmospheric range as a function of sky irradiance, filter bandwidth and transmission and laser transmitted UV energy.

15. SUBJECT TERMS

Lidar; Lidar receiver; Ozone; Range

16. SECURITY CLASSIFICATION OF:			17. LIMITATION OF ABSTRACT	18. NUMBER OF PAGES	19a. NAME OF RESPONSIBLE PERSON
a. REPORT	b. ABSTRACT	c. THIS PAGE			STI Help Desk (email: help@sti.nasa.gov)
					19b. TELEPHONE NUMBER *(Include area code)*
U	U	U	UU	22	(443) 757-5802